# Modelling and Analysis of Permanent Magnet Electrodynamic Suspension Systems

**Hossein Rezaei and Sadegh Vaez-Zadeh**[*]

**Abstract**—In this paper, an analytical model of permanent magnet electrodynamic suspension systems (PEDSs) is proposed. Horizontal and vertical magnetic fields of a permanent magnet (PM) are effectively approximated by sinusoidal functions. By this means, closed form solutions are obtained for lift and drag forces of PEDSs for the first time. The suspension system is then modelled by finite element method (FEM). The accuracy of the analytical model is validated by FEM and experimental measurements.

## 1. INTRODUCTION

Nowadays electrodynamic suspension (EDS) systems have different applications in rapid transportation, magnetic bearing, space launchers, etc. Utilization of permanent magnet in EDS has gained increasing attention due to several merits. It does not need power sources, superconductor coils and complicated systems. It is found that lift and drag forces are influenced by magnetic field distribution, induced eddy currents and their interactions. Detailed and effective studies of parameter impact on lift and drag forces need accurate and simple analytical models for investigating these forces.

Modelling of electrodynamic bearing based on computation of electromagnetic force is presented and compared with experimental results [1]. Computation of magnetic field, eddy current and developed forces of an electrodynamic levitation device by finite volume method modelling caused reduction of storage memory and computation time [2]. Lift and thrust or braking forces in translating and rotating electodynamic wheels are modeled by 2D steady state FEM [3]. Lift and drag forces of a suspension system with Halbach arrays are analyzed by 2D FEM and experimental measurements [4]. The lift and drag forces of two EDS systems with flat and cylindrical conducting sheet are studied and compared by finite element method [5]. The effect of conducting sheet thickness, airgap and PM dimensions on the PEDS performance is also investigated [6]. Since the numerical analysis is time-consuming, it is not adequate for design and optimization purposes. Such an analysis can evaluate only a final design of the suspension system.

Coil induced current distribution of an EDS that consists of superconductor magnets above a split guideway conductor is obtained based on the dynamic circuit theory [7]. An analytical model for magnetic fields, eddy currents and developed forces for PMs above a continuous conducting sheet are obtained. However, closed form equations of lift and drag forces are not given. Equations of lift and drag forces for electromagnet with sinusoidal current distribution are presented [8, 9]. In EDS with halbach arrays, lift and drag forces are obtained by Lorentz law [10]. However, they are not applicable to EDS systems with conventional PM.

In this paper an analytical model of lift and drag forces for PEDS in terms of system parameters is found. Observations of magnetic field around PM show that magnetic fields vary quasi-sinusoidal with respect to longitudinal movement. Therefore, only fundamental components of magnetic fields are considered. They are calculated by modeling PM as current sheets. Also, lift and drag forces

* Corresponding author: Sadegh Vaez-Zadeh (vaezs@ut.ac.ir).
The authors are with the Center of Excellence on Applied Electromagnetic Systems and Advanced Motion Systems Research Laboratory, School of Electrical and Computer Engineering, University of Tehran, Tehran, Iran.

are obtained in terms of EDS parameters. Finally, analytical results are confirmed by 2D FEM and experimental results.

## 2. PHYSICAL MODEL

A Physical model of EDS is depicted in Fig. 1. This figure shows that a PM with a length $L$ and a height $D$ moves at the velocity of $V_x$ with respect to a conducting sheet with a thickness $d$ and a conductivity $\sigma$. PM magnetic field varies from the view point of conducting sheet. This induces an eddy current in the sheet which in turn repels the PM. Moving the PM along the positive direction of $x$ axis develops a drag force along $-x$ direction and lift force at $+y$ direction.
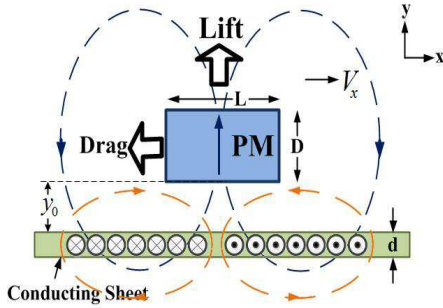


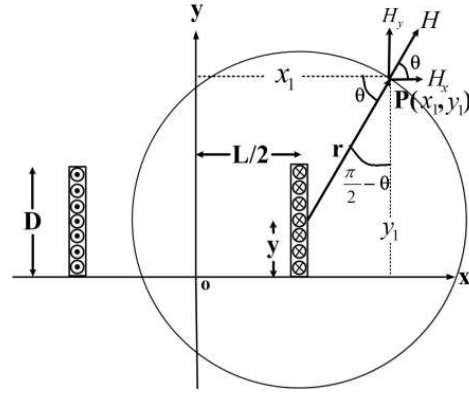**Figure 1.** Physical model of electo-dynamic suspension system.



**Figure 2.** Modeling of PM by current sheets.

## 3. FIELD AND FORCE ANALYSIS

The PM with uniform magnetization can be modeled by two current sheets at PM ends as seen in Fig. 2. Magnetic field and its variations are considered only in $x$ and $y$ directions. By assuming infinite current sheets in $\pm z$ direction, magnetic field and its variations in $z$ direction are ignored and the calculations are carried out for a unit depth. The current sheet density and the magnetization of PM can be calculated as $J_{SZ} = M_0 \hat{a}_z$ where $M_0 = \frac{B_{rm}}{\mu_0}$ and $B_{rm}$ stands for PM residual flux density and $\mu_0$ for air permeability. The magnetic field at point $P(x_1, y_1)$ can be written as $\partial H = \frac{\partial I}{2\pi r}$ where $\partial I = M_0 \partial y$ and

$$r = \sqrt{\left(x_1 - \frac{L}{2}\right)^2 + (y_1 - y)^2} \tag{1}$$

The magnetic field due to the current sheet can be decoupled into a horizontal-component and a vertical-component. These components can be calculated by $\partial H_x = \partial H \cos(\theta)$ and $\partial H_y = \partial H \sin(\theta)$.

According to Fig. 2 $\sin(\theta)$ and $\cos(\theta)$ can be obtained as:

$$\sin(\theta) = \frac{y_1 - y}{\sqrt{\left(x_1 - \frac{L}{2}\right)^2 + (y_1 - y)^2}} \tag{2}$$

$$\cos(\theta) = \frac{x_1 - \frac{L}{2}}{\sqrt{\left(x_1 - \frac{L}{2}\right)^2 + (y_1 - y)^2}} \tag{3}$$

The total horizontal and vertical magnetic fields at any point are provided by the current sheets at $x = -L/2$ and $x = L/2$. Therefore, the PM magnetic fields are obtained by integrating their derivatives,

mentioned above, over the current sheets. As a result, the horizontal and vertical magnetic fields around a PM can be written as:

$$
\begin{aligned}
H_x &= \int_0^D \frac{M_0(y_1 - y)dy}{2\pi\left(\left(x_1 - \frac{L}{2}\right)^2 + (y_1 - y)^2\right)} - \int_0^D \frac{M_0(y_1 + y)dy}{2\pi\left(\left(x_1 + \frac{L}{2}\right)^2 + (y_1 - y)^2\right)} \\
&= \frac{M_0}{4\pi}\left[\log\left(\frac{\left(x_1 - \frac{L}{2}\right)^2 + (y_1)^2}{\left(x_1 - \frac{L}{2}\right)^2 + (y_1 - D)^2}\right) - \log\left(\frac{\left(x_1 + \frac{L}{2}\right)^2 + (y_1)^2}{\left(x_1 + \frac{L}{2}\right)^2 + (y_1 - D)^2}\right)\right]
\end{aligned} \tag{4}
$$

$$
\begin{aligned}
H_y &= \int_0^D \frac{M_0\left(x_1 - \frac{L}{2}\right)dy}{2\pi\left(\left(x_1 - \frac{L}{2}\right)^2 + (y_1 - y)^2\right)} - \int_0^D \frac{M_0\left(x_1 + \frac{L}{2}\right)dy}{2\pi\left(\left(x_1 + \frac{L}{2}\right)^2 + (y_1 - y)^2\right)} \\
&= \frac{M_0}{2\pi}\left[-\tan^{-1}\left(\frac{(y_1 - D)}{x_1 - \frac{L}{2}}\right) + \tan^{-1}\left(\frac{(y_1)}{x_1 - \frac{L}{2}}\right) + \tan^{-1}\left(\frac{(y_1 - D)}{x_1 + \frac{L}{2}}\right) - \tan^{-1}\left(\frac{(y_1)}{x_1 + \frac{L}{2}}\right)\right]
\end{aligned} \tag{5}
$$

It should be mentioned that the model may not be accurate enough when the PM magnetization curve is nonlinear. Also, the model is not valid when the PM has limited depth with respect to other PM dimensions. Horizontal and vertical magnetic fields of a neodymium PM with dimensions of 45 mm×5 mm in a 5 mm airgap are indicated in Figs. 3 and 4. It is seen that PM magnetic field variations due to harmonics of the magnetic fields do not contribute much to the effective forces. Therefore, only the fundamental component of the fields are considered in force calculations. Fundamental harmonics of horizontal and vertical magnetic field are also indicated in Fig. 3. If a PM develops vertical and horizontal magnetic fields that vary sinusoidally with respect to longitudinal movement, fields magnitudes decrease exponentially with respect to distance from PM. Therefore, horizontal and vertical magnetic field can be obtained as [8, 9]:

$$
H_x = -h_x \sin\left(\frac{\pi x}{L}\right)e^{-\frac{\pi y}{L}} \tag{6}
$$

$$
H_y = h_y \cos\left(\frac{\pi x}{L}\right)e^{-\frac{\pi y}{L}} \tag{7}
$$

By increasing the PM length with regard to distance from PM, the magnetic field sensitivity with respect to PM distance decreases. The magnetic field decay is negligible for $L \geq 100\pi y_0$. In the current EDS system, the magnet length is not much higher than the distance. Therefore, the distance is considered by $e^{-\frac{2\pi y_0}{L}}$ factor in (8) and (9). Magnetic fields and their variations in $z$ direction are ignored and conductor sheet is supposed to be thin with respect to eddy current depth. As a result, the developed lift and drag forces per unit depth are described by (8) and (9) [8]:

$$
F_L = 2\mu_0 L h_x h_y e^{-\frac{2\pi y_0}{L}} \frac{V_x^2}{V_x^2 + w^2} \tag{8}
$$

$$
F_D = 2\mu_0 w L h_y^2 e^{-\frac{2\pi y_0}{L}} \frac{V_x}{V_x^2 + w^2} \tag{9}
$$

where $w$ can be obtained as $w = \frac{2}{\mu_0 \sigma d}$. It is noted that $h_x$ and $h_y$ are the coefficients of fundamental components of horizontal and vertical magnetic fields, respectively. The components are also depicted with respect to longitudinal movement in Figs. 3 and 4.

For the PM with a finite thickness much smaller than its length, each current sheets at PM ends can be considered as a single sheet as indicated in Fig. 5. In this case, the current sheet density is replaced by $M_0 D$. Also, if fundamental component of vertical and horizontal magnetic fields are the same, $h_x$ and $h_y$ can be calculated as:

$$
h_x = H_x\left(x = -\frac{L}{2}, y = 0\right) = h_y = H_y(x = 0, y = 0) = H \tag{10}
$$

The magnetic field due to current sheet 1 at the point $P(r, \theta)$ in Fig. 3, can be written as:

$$
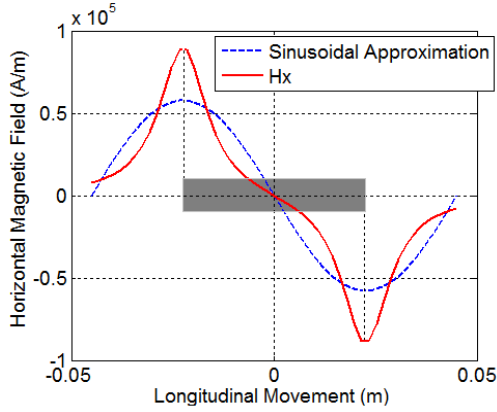H_{1p}(r, \theta) = \frac{M_0 D}{2\pi r} \tag{11}
$$

**Figure 3.** Horizontal magnetic field and its fundamental component.
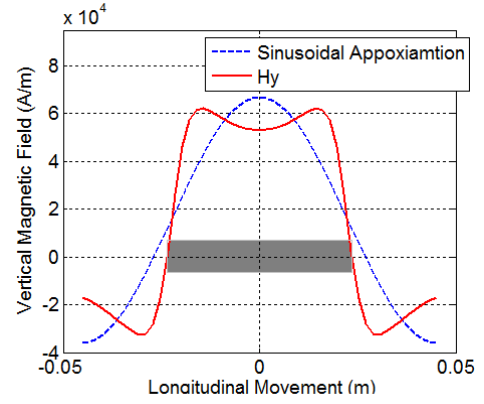


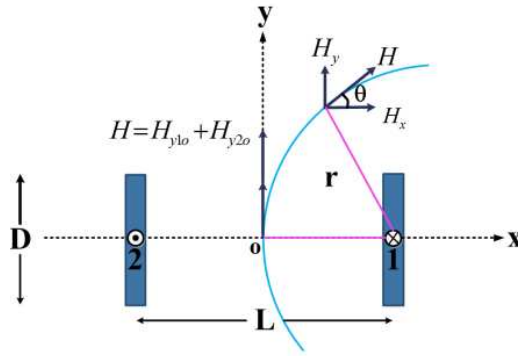**Figure 4.** Vertical magnetic field and its fundamental component.



**Figure 5.** Model of PM by single current sheet.

According to Fig. 3, horizontal and vertical components of $H_{1p}$ are obtained as:

$$H_{x1p}(r, \theta) = \frac{M_0 D}{2\pi r} \cos(\theta) \tag{12}$$

$$H_{y1p}(r, \theta) = \frac{M_0 D}{2\pi r} \sin(\theta) \tag{13}$$

Vertical magnetic field due to current sheet 1 at the point $o\left(L/2, \pi/2\right)$ is given as:

$$H_{y10}\left(\frac{L}{2}, \frac{\pi}{2}\right) = \frac{M_0 D}{2\pi \left(\frac{L}{2}\right)} = \frac{M_0 D}{\pi L} \tag{14}$$

The model is particularly accurate when the PM thickness is shorter PM length. Net vertical magnetic field at the point $o(L/2, \pi/2)$ can be obtained as:

$$H = H_{y10} + H_{y20} = \frac{2M_0 D}{\pi L} \tag{15}$$

Since $H$ is obtained at the center of PM, $y_0$ in (8) and (9) is placed by $y_0 + D/2$. The lift and drag forces per unit depth in terms of system parameters is given by substituting (10), (11) and (15) into (8) and (9):

$$F_L = \frac{8\mu_0 \left(M_0 D\right)^2}{\pi^2 L} e^{\frac{-2\pi\left(y_0 + \frac{D}{2}\right)}{L}} \frac{V_x^2}{V_x^2 + w^2} \tag{16}$$

$$F_D = \frac{8w\mu_0 \left(M_0 D\right)^2}{\pi^2 L} e^{\frac{-2\pi\left(y_0 + \frac{D}{2}\right)}{L}} \frac{V_x}{V_x^2 + w^2} \tag{17}$$

## 4. FEM VALIDATION

### 4.1. Finite Element Method

In this section, 2-D FEM is used to evaluate the force calculations. The PM movement is taken into account by using time-stepping analysis. Lift and drag forces are computed by using Maxwell stress tensor method. In Maxwell stress tensor method, vertical and horizontal forces at the path $dl$ are obtained by:

$$dF_n = \frac{B_n B_t}{M_0} dl \tag{18}$$

$$dF_t = \frac{B_n^2 - B_t^2}{2M_0} dl \tag{19}$$

The force are calculated on surfaces of air elements. The method extrapolates field values. Electromagnetic forces are calculated according to the virtual work principle. A schematic view of PEDS model is shown in Fig. 6. Also, mesh generation of the PEDS model is shown in Fig. 7. This consists of two parts. The first part in the motion band has fine meshes. The second part includes the region far from the motion band. The zero vector potential is used for boundary conditions of the FEM model. The solution method is of transient type.
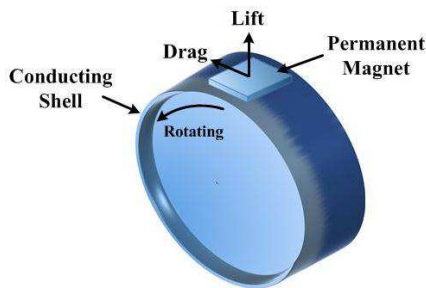


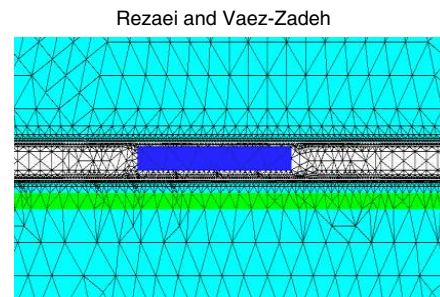**Figure 6.** Schematic view of PEDS system.



**Figure 7.** Mesh generation of PEDS model.

### 4.2. FEM Results

Magnetic flux paths and magnetic field spectrum are indicated in Figs. 8 and 9 respectively. It is seen that magnetic field has greater magnitude beside PM pole and decreases at the middle of PM. The analytical relationships obtained for lift and drag forces are evaluated in thin section by FEM modeling of the PEDS. 2D FEM and analytical results of lift and drag forces in terms of velocity are illustrated in Fig. 10 which are close to each other. However, there is a little difference between analytical and FEM results. The reasons is as follows:
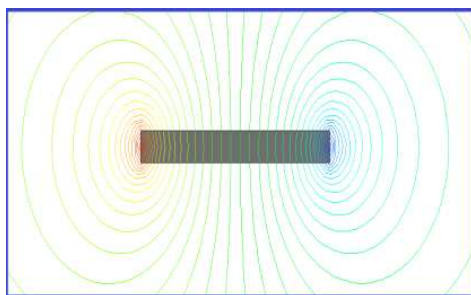


**Figure 8.** Magnetic flux paths around the PM.
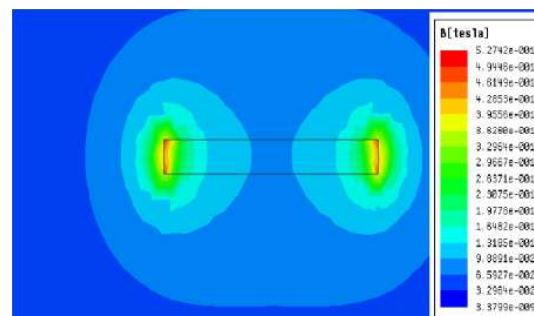


**Figure 9.** Magnetic field spectrum around the PM.

1. In analytical equations, it is assumed that $J_z$ does not vary in regards to vertical direction. This assumption is valid when the sheet thickness is small with respect to eddy current depth. But at high velocities, this assumption is not valid in FEM analysis.
2. Magnetic field distribution along with the PM length has sinusoidal harmonics that affects lift and dag force development. But analytical relationships do not regard magnetic field harmonics.
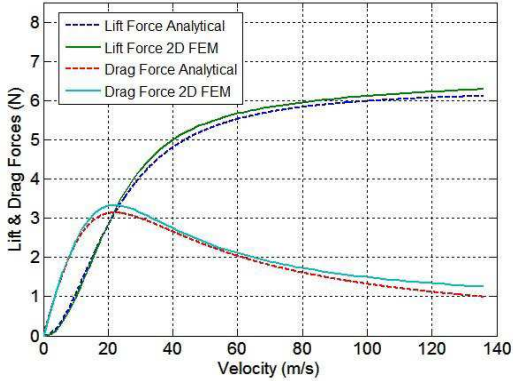


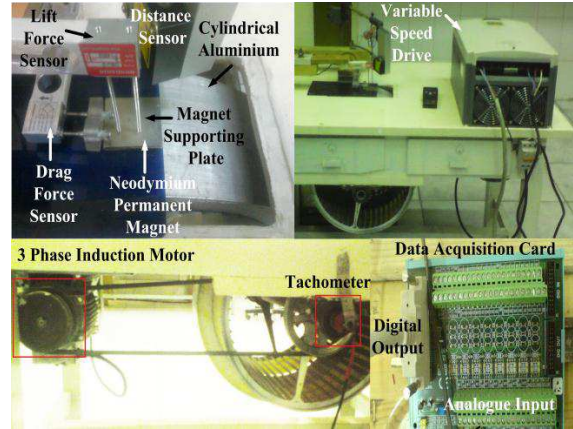**Figure 10.** Lift and drag forces in terms of velocity.



**Figure 11.** Experimental PEDS system.

## 5. EXPERIMENTAL VALIDATION

### 5.1. Experimental System

A permanent magnet suspension system consisting of a PM block, a rotating cylindrical Al shell and measuring instruments is used for experimental evaluation. A photo of experimental set-up is shown in Fig. 11. The way of using distance, force, and speed sensors and also the arrangement of the
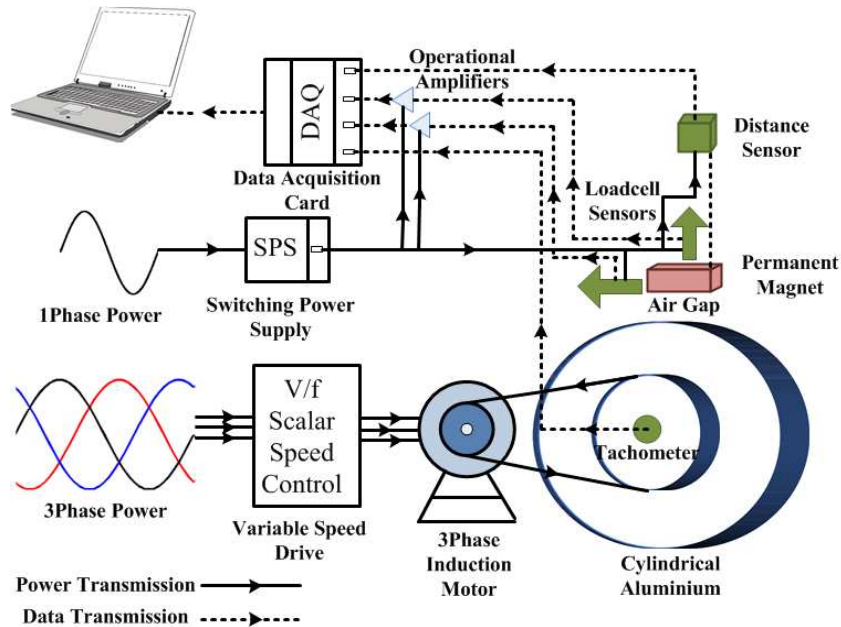


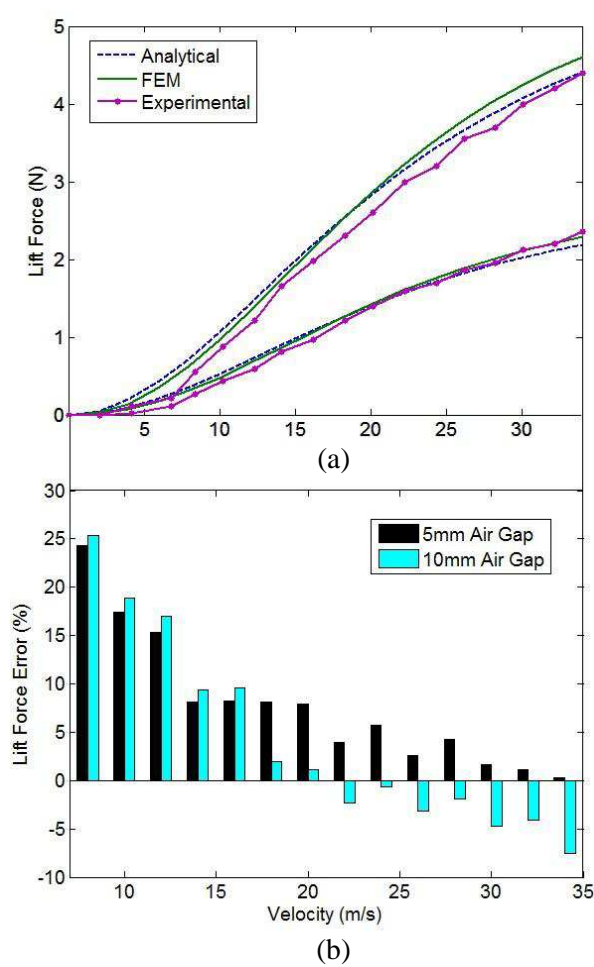**Figure 12.** Schematic view of experimental system.

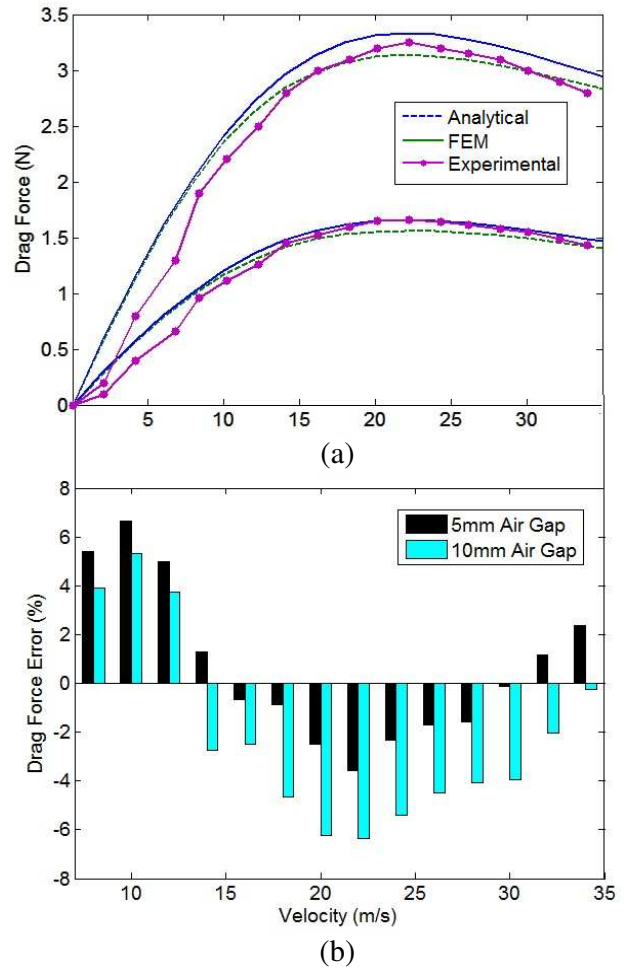**Figure 13.** Lift force; (a) Value, (b) error.



**Figure 14.** Drag force; (a) Value, (b) error.

connection of other equipment are shown in Fig. 12. Rotating speed, lift and drag forces are measured by a tachometer and loadcells, respectively. Output signals of loadcells are amplified by operational amplifiers. In this figure, solid and dashed lines show power and data transmissions respectively. A three-phase power supply is connected to a variable speed drive that rotates AL cylinder. Also, a switching power supply connected to a single phase main to provide a 12-V DC voltage for sensors and amplifier. The output of sensors are amplified and sent to a personal computer to be analyzed. FEM, analytical and experimental results of lift and drag forces in terms of velocity are illustrated in Figs. 13 and 14.

## 5.2. Test Results

Comparison of FEM, analytical and experimental outcome show good agreement of the results. This validates the analytical model and the given lift and drag relationships. However a little discrepancy can be seen between the analytical results and test results. This may be provided by

1. In analytical and FEM modeling of suspension system, the magnetic field and its variation in $z$ direction are neglected and lift and drag forces are obtained by 2D FEM. Infinite PM depth in FEM modelling causes to decrease accuracy of 2D modeling.

2. The conducting sheet of experimental system is a cylindrical aluminum shell, but in analytical and FEM modeling, a flat conducting sheet is considered.

## 6. CONCLUSION

In this paper, analytical solutions for lift and drag forces of PEDS are presented. They are achieved by considering fundamental component of both horizontal and vertical magnetic fields and obtained by a straightforward physical model of permanent magnets. Permanent magnet length and thickness show conflicting effects on both lift and drag forces providing an opportunity for optimizing magnet dimensions for achieving high forces. Analytical results of lift and drag forces are compared with FEM and experimental results. They validate the accuracy of the analytical modeling of EDS systems and justifies its application in the design optimization.

## APPENDIX A. SYSTEM SPECIFICATION

Aluminum Conductivity: $3.85 * 10^7$ S/m; Neodymium Coercive Force: 838 KA/m; Neodymium Permeability: 1.0000004; Air Permeability: 1.045; Aluminum Permeability: 1.000021.

## REFERENCES

1. Impinna, F., J. G. Detoni, N. Amati, and A. Tonoli, "Passive magnetic levitation of rotors on axial electodynamic bearings," *IEEE Transactions on Magnetics*, Vol. 49, 599–608, 2013.
2. Mabrouk, A. E., A. Cheriet, and M. Feliachi, "Fuzzy logic control of electrodynamic levitation devices coupled to dynamic finite volume method analysis," *Applied Mathematical Modelling*, Vol. 37, 5951–5961, Apr. 15, 2013.
3. Paudel, N., J. Bird, S. Paul, and D. Bobba, "A transient 2D model of an electrodynamic wheel moving above a conductive guideway," *2011 IEEE International Electric Machines* & *Drives Conference (IEMDC)*, 545–550, 2011.
4. Íñiguez, J. and V. Raposo, "Numerical simulation of a simple low-speed model for an electrodynamic levitation system based on a Halbach magnet array," *Journal of Magnetism and Magnetic Materials*, Vol. 322, 1673–1676, 2010.
5. Najjar-Khodabakhsh, A., S. Vaez-Zadeh, and A. H. Isfahani, "Finite element analysis and experimental implementation of the cylindrical permanent magnet electrodynamic suspension system," *Electromagnetics*, Vol. 29, 563–574, Sep. 29, 2009.
6. Najjar-khodabakhsh, A., S. Vaez-Zadeh, and A. Hassanpour Isfahani, "Analysis of a cylindrical passive suspension system using finite element method," *Int. Rev. of Elect. Eng. (IREE)*, Vol. 3, No. 1, 123–128, Jan. 2008.
7. Sakamoto, T., A. R. Eastham, and G. E. Dawson, "Induced currents and forces for the split-guideway electrodynamic levitation system," *IEEE Transactions on Magnetics*, Vol. 27, 5004–5006, 1991.
8. Hill, R. J., "Teaching electrodynamic levitation theory," *IEEE Transactions on Education*, Vol. 33, 346–354, 1990.
9. Post, R. F. and D. D. Ryutov, "The inductrack: A simpler approach to magnetic levitation," *IEEE Transactions on Applied Superconductivity*, Vol. 10, 901–904, 2000.
10. Sugimoto, H. and A. Chiba, "Stability consideration of magnetic suspension in two-axis actively positioned bearingless motor with collocation problem," *IEEE Transactions on Industry Applications*, Vol. 50, 338–345, 2014.